



## Short communication

# Superior cycle stability of graphene nanosheets prepared by freeze-drying process as anodes for lithium-ion batteries



Dandan Cai<sup>a</sup>, Suqing Wang<sup>a,\*</sup>, Liangxin Ding<sup>a</sup>, Peichao Lian<sup>b</sup>, Shanqing Zhang<sup>c</sup>,  
Feng Peng<sup>a</sup>, Haihui Wang<sup>a,\*</sup>

<sup>a</sup> School of Chemistry & Chemical Engineering, South China University of Technology, Wushan Road, Guangzhou, China

<sup>b</sup> Faculty of Chemical Engineering, Kunming University of Science and Technology, Kunming 650500, China

<sup>c</sup> Centre for Clean Environment and Energy, Environmental Futures Centre, and Griffith School of Environment, Gold Coast Campus, Griffith University, QLD 4222, Australia

## H I G H L I G H T S

- A novel facile synthesis of graphene nanosheets involving freeze-drying technology.
- The as-prepared materials exhibit superior cycle stability and rate performance.
- The freeze-drying helps to enlarge the interlayer distance and specific surface area.

## A R T I C L E I N F O

## Article history:

Received 27 November 2013

Received in revised form

27 December 2013

Accepted 31 December 2013

Available online 8 January 2014

## Keywords:

Graphene nanosheets

Freeze-drying

Cycle stability

Anode materials

Lithium-ion batteries

## A B S T R A C T

Graphene nanosheets are synthesized by a novel facile method involving freeze-drying technology and thermal reduction. The microstructure and morphologies are characterized by X-ray diffraction, Brunauer–Emmett–Teller measurements, Fourier transform infrared spectroscopy, and high resolution transmission electron microscope. The results indicate that graphene nanosheets with high specific surface area ( $358.3 \text{ m}^2 \text{ g}^{-1}$ ) and increased interlayer distance ( $0.385 \text{ nm}$ ) are successfully obtained through the freeze-drying process. The electrochemical performances are evaluated by using coin-type cells versus lithium. A high initial reversible capacity of  $1132.9 \text{ mAh g}^{-1}$  is obtained at a current density of  $100 \text{ mA g}^{-1}$ . More importantly, even after 300 cycles at a high current density of  $1000 \text{ mA g}^{-1}$ , a stable specific capacity of  $556.9 \text{ mAh g}^{-1}$  can be achieved, suggesting the graphene nanosheets exhibit superior cycle stability. The fascinating electrochemical performance could be ascribed to the high specific surface area and the increased layer distance between the graphene nanosheets.

© 2014 Elsevier B.V. All rights reserved.

## 1. Introduction

Lithium-ion batteries (LIBs) are the most attractive secondary batteries because of their high energy density, relatively low self-discharge, zero memory effect and excellent safety. Graphene, as a promising anode material for LIBs, has attracted much attention in the recent years due to its superior electronic conductivity, intriguing mechanical properties, and high reversible capacity [1–8]. But graphene still suffers from poor cycling stability and a low specific capacity at high current density, which restricts it from large-scale practical applications. Also graphene nanosheets can easily restack with each other, leading to the loss of the features of graphene [9]. In

order to solve the problems, various attempts have been made, such as incorporation of nanotubes or fullerenes [1], design of porous structure [10–14], and introduction of dopants and defects [15–20]. However, most of the above-mentioned modification methods involve complicated and time-consuming production process, which is not economically viable for mass production. Thus, simple, mild and low cost processes are desirable for the preparation of the graphene materials with high electrochemical performance.

Freeze-drying method has been considered to be a simple and efficient approach to retain the microstructure and specific surface area of the treated samples during the drying process. It can be used to create porous structures of nanomaterials [21–24]. In particular, nitrogen and boron co-doped graphene aerogel prepared by freeze-drying technology is applied to the all-solid-state supercapacitors and shows excellent electrochemical performance [25]. This is mainly ascribed to the three-dimensional porous structure with

\* Corresponding authors. Tel./fax: +86 20 87110131.

E-mail addresses: [cesqwang@scut.edu.cn](mailto:cesqwang@scut.edu.cn) (S. Wang), [hhwang@scut.edu.cn](mailto:hhwang@scut.edu.cn) (H. Wang).

high specific surface area formed in the freeze-drying process. In addition, the freeze-drying method is also considered as a promising synthetic way to prepare cathode materials for LIBs [26,27]. Moreover, graphene-based materials obtained through the freeze-drying process exhibited excellent rate performance and cycling stability [28–30]. For instance, a  $\text{SnO}_2$  nanocrystal/nitrogen-doped reduced graphene oxide nanocomposite prepared and dried by the freeze-drying process demonstrated a reversible capacity of  $1346 \text{ mAh g}^{-1}$  after 500 cycles [30]. However, it is rarely reported that the freeze-drying technology were utilized as a synthetic tool to create nanostructures of graphene materials, especially the lyophilisation effect on structure and physicochemical properties of the graphene materials.

Herein, graphene nanosheets were synthesized by freezing-drying technology followed by thermal reduction. The characterizations and electrochemical performances of the graphene nanosheets obtained by freeze-drying process (denoted as FGNs) and rotary evaporation process (denoted as RGNs) were investigated and compared. The as-prepared FGNs as anode materials for LIBs are expected to show a superior cycle stability and excellent rate performance.

## 2. Experimental section

### 2.1. Synthesis of the FGNs and the RGNs

The FGNs were synthesized by freeze-drying and thermal reduction process from graphite oxides. Graphite oxides were prepared through the modified Hammer's method. Detailed preparation procedure can be found in our previous report [6]. Typically, the as-prepared graphite oxides were dispersed in deionized water by the ultrasound wave to form the graphene oxides. Then, the dispersion graphene oxides aqueous solution was frozen and the ice crystal was sublimated by vacuum freeze-drying. Finally, the as-prepared freeze-dried-material was thermally reduced at  $800^\circ\text{C}$  in argon gas atmosphere and then the FGNs were obtained. For comparison, the RGNs were prepared under the same condition using the rotary evaporation process instead of the freeze-drying process.

### 2.2. Materials characterization

The morphology and structure of the FGNs and the RGNs were characterized by X-ray diffraction (XRD) patterns from PHILIPSPW1710 using  $\text{Cu/K}\alpha$  radiation. The specific surface area was measured using the Brunauer–Emmett–Teller (BET) method (Micromeritics analyzer ASAP 2020 (USA)) at liquid nitrogen temperature. The information of functional groups was measured by Fourier transform infrared spectroscopy instrument (FTIR, Bruker Vector 33). The structure and morphology were characterized by the high resolution transmission electron microscope (HRTEM) (JEM-2010HR).

### 2.3. Electrochemical measurements

The electrochemical performances were investigated using coin-type half cells. The working electrodes were prepared by coating the slurry of the active materials (80 wt.%), Super P (10 wt.%), and poly(vinylidene fluoride) (PVDF) (10 wt.%) dissolved in an *N*-methyl-2-pyrrolidone (NMP) solvent onto a copper foil and dried in a vacuum oven at  $100^\circ\text{C}$ . Lithium metal was utilized as a counter electrode while the celgard 2325 membrane was used as a separator. The electrolyte was  $1 \text{ mol L}^{-1} \text{ LiPF}_6$  in a mixture solution of ethylene carbonate (EC) and diethylcarbonate (DEC) (1:1 by volume). The CR2025 type coin cells were used as testing batteries

and assembled in an argon-filled glove box where the oxygen and moisture contents were less than 1 ppm.

The cells were galvanostatically discharged and charged using a Battery Testing System (Neware Electronic Co., China) between 0.01 and 3.0 V at different current densities. Cyclic voltammetry (CV) measurements were carried out on an electrochemical workstation (Zahner IM6ex) over the potential range of 0.01–3.0 V vs.  $\text{Li/Li}^+$  at a scanning rate of  $0.2 \text{ mV s}^{-1}$ . Electrochemical impedance spectra (EIS) of the FGNs and RGNs before cycling and after 3 cycles at the current density of  $100 \text{ mA g}^{-1}$  were measured utilizing an electrochemical workstation (Zahner IM6ex). The frequency range was set from 10 mHz to 100 KHz and the potential amplitude was 5 mV.

## 3. Results and discussion

### 3.1. Materials characterization

XRD patterns of the FGNs and the RGNs are shown in Fig. 1. For FGNs, it is found that a typical weak dispersive and wide (002) diffraction peak at  $25.11^\circ$  is observed, suggests that interlayer distance of nanosheets is large, which is consistent with the previously reported graphene materials [2,3,6]. In strong contrast, the (002) diffraction peak of the RGNs becomes much sharper and more intense, suggesting that the interlayer distance of the graphene nanosheets is small and the restacking of the graphene nanosheets is serious during the rotary evaporation process [2]. The results indicate that the freeze-drying technology may significantly minimize the restacking of graphene nanosheets.

HRTEM was used to characterize the structure and the interlayer distance of the FGNs and the RGNs. As shown in Fig. 2a, the FGNs are entangled with each other and formed wrinkled paper-like structure. The typical wrinkled structure with corrugation and scrolling is similar to the previous reports [31,32]. Fig. 2b exhibits the interlayer distance between the graphene nanosheets in the HRTEM cross section. The interlayer distance was measured to be 0.385 nm, which is larger than that of graphite (0.335 nm). In order to demonstrate the role of freeze-drying process, HRTEM images of the RGNs were also shown in Fig. 2c and d. It indicates that the graphene nanosheets of the RGNs sample are seriously stacked with each other, which is in agreement with the XRD results. What's more, it is difficult to distinguish the layer distance of the RGNs because of the formation of the stacked graphene nanosheets. The increased layer distance between graphene nanosheets for the FGNs suggests that the interlayer distance is influenced by the

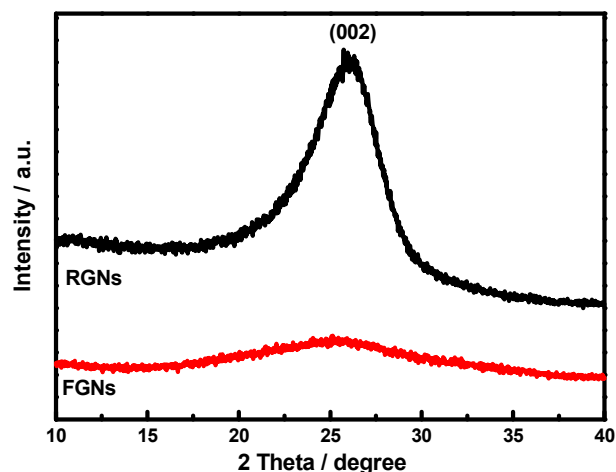


Fig. 1. XRD patterns of the FGNs and the RGNs.

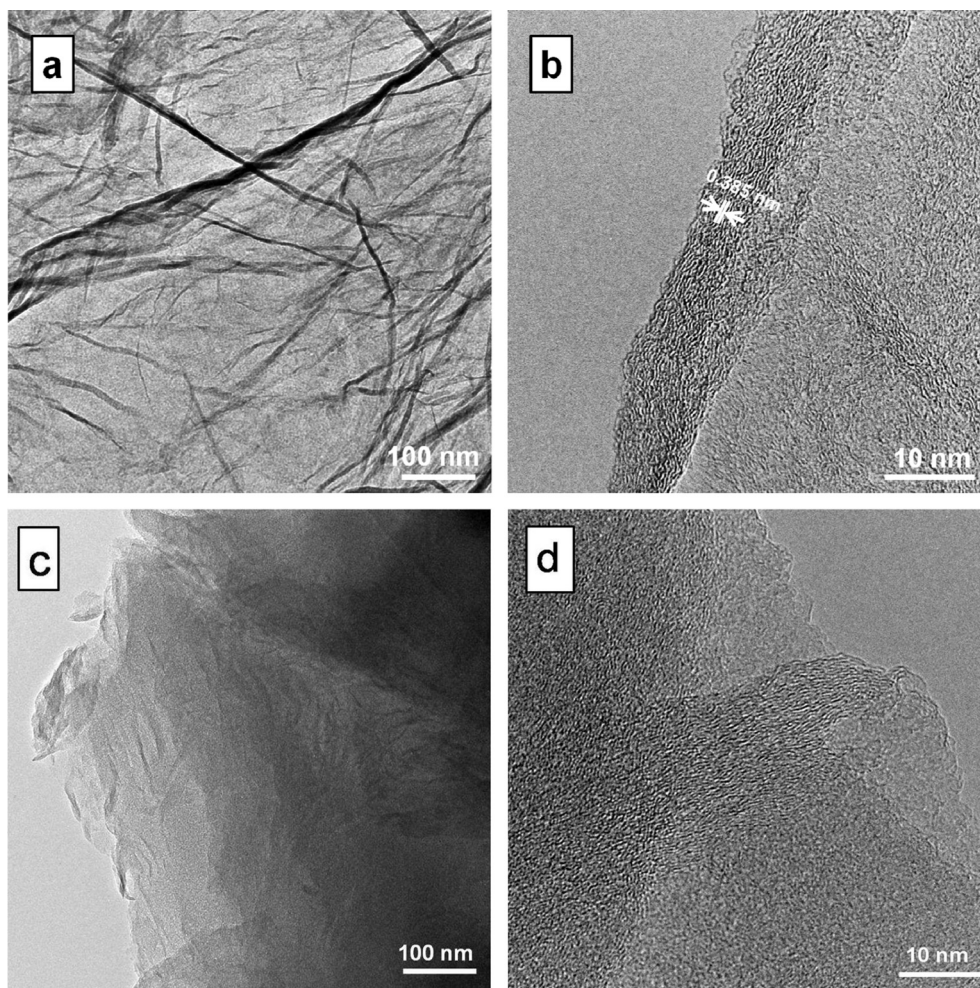


Fig. 2. HRTEM images of (a, b) the FGNs and (c, d) the RGNs.

freeze-drying process, and the possible explanation was described as follows. Graphene oxide sheets are considered to be hydrophilic sheets due to the abundant surface functional groups on the sheets [33,34]. The graphene oxides aqueous solution was frozen and as a result ice crystals are stuffed into the interspacing between graphene interlayer to increase the space distance. When the ice crystal was sublimated under high vacuum in the freeze-drying process, the increased interlayer distance is retained [21,22]. As a result, the as-obtained large layer distance could provide more lithium storage sites for graphene nanosheets electrode during the discharge/charge process [1]. The TEM images suggest the freeze-drying process plays an important role in prevention of the restacking and expansion of interlayer distance of the graphene.

The nitrogen adsorption–desorption isotherms of the FGNs and the RGNs are shown in Fig. 3a. The BET specific surface area of the FGNs is calculated to be  $358.3 \text{ m}^2 \text{ g}^{-1}$ , which is much higher than that of the RGNs ( $14 \text{ m}^2 \text{ g}^{-1}$ ) and that of previously reported graphene nanosheets ( $184 \text{ m}^2 \text{ g}^{-1}$ ) [3]. Moreover, a typical IV-type hysteresis loop in the nitrogen adsorption/desorption isotherms of the FGNs was also observed, which indicates that the FGNs has form a porous structure [35,36]. Such porous structure could facilitate the ultra-fast transportation of lithium ions during the cycling process, which may improve the rate performance of lithium-ion batteries [37,38]. The pore distribution curve of the FGNs was derived by the density functional theory (DFT) method. The majority pore sizes of 1.3 and 3.2 nm can be clearly observed from the pore size

distribution curve (inset of Fig. 3a). The FTIR spectra of the graphene oxides, RGNs and FGNs are shown in Fig. 3b. For the precursor-graphene oxides, a lot of surface functional groups are observed, such as O–H stretch at  $3390 \text{ cm}^{-1}$ , C=O stretch at  $1733 \text{ cm}^{-1}$ , and C–O stretch at  $1056 \text{ cm}^{-1}$ . However, for the RGNs and FGNs, the C–O and C=O stretches becomes almost indistinguishable after the thermal treatment. Moreover, the peak at about  $3440 \text{ cm}^{-1}$  and  $1638 \text{ cm}^{-1}$  can be attributed to O–H stretching vibrations and bending vibrations of adsorbed water molecules or structural OH groups, respectively. The result indicates that most of the surface functional groups of both RGNs and FGNs are removed by the thermal reduction, which is consistent with the previous reports [2,3,6].

### 3.2. Electrochemical properties of the FGNs and the RGNs

Fig. 4a presents the cyclic voltammograms of the as-prepared FGNs anode at a scanning rate of  $0.2 \text{ mV s}^{-1}$ . The shape of the cyclic voltammograms is well consistent with the discharge/charge profiles (Fig. 4b) and the previous report [4]. As shown in Fig. 4a, a prominent peak located at about 0.6 V at first cycle is related to the solid-electrolyte-interphase (SEI) films formed on the surface of the anode. A peak closed to 0 V was also observed, which is attributed to lithium ions intercalation into the carbon-based anodes [4,6]. More interestingly, the similarity in the second and the third cycles for the as-prepared FGNs suggests that the materials show high reversibility of the electrochemical reactions.

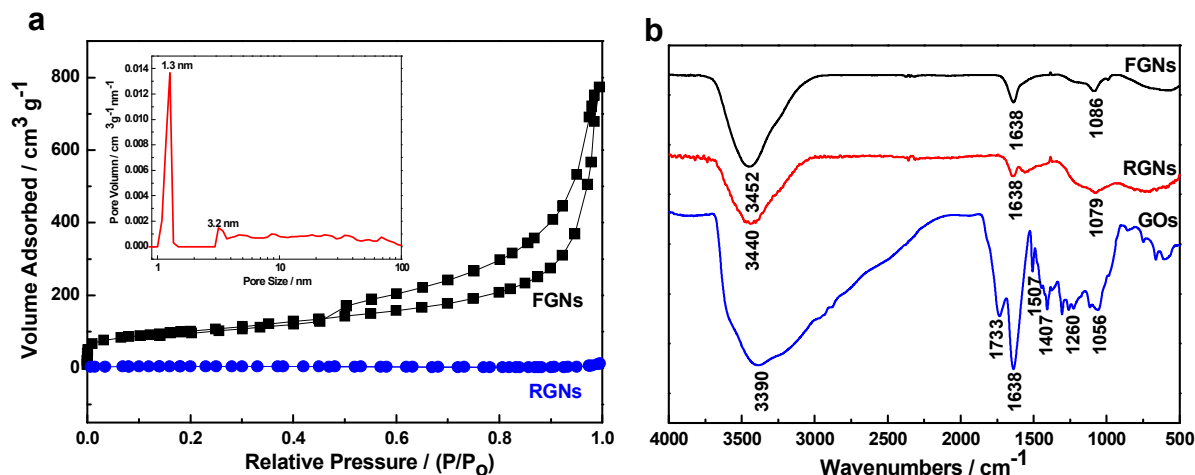


**Fig. 3.** (a) Nitrogen adsorption/desorption isotherm of the FGNs and the RGNs. Inset: pore-size distribution plot of the graphene nanosheets calculated using the DFT method. (b) FTIR spectra of graphene oxides (GOs), RGNs and FGNs.

Fig. 4b shows the initial discharge/charge profiles of the FGNs and the RGNs at a current density of  $100 \text{ mA g}^{-1}$ . The discharge/charge curves of the FGNs displayed similar profiles as those of the previous reports [1–8]. Furthermore, for the FGNs, a high reversible capacity of  $1132.9 \text{ mAh g}^{-1}$  was obtained at a current density of  $100 \text{ mA g}^{-1}$ . Obviously, the reversible capacity of the FGNs is far higher than that of the RGNs ( $391 \text{ mAh g}^{-1}$ ). The as-obtained high reversible capacity might be related to the high specific surface area and the increased interlayer distance between graphene nanosheets [1,10,12,13].

The cycling stabilities of the FGNs and RGNs at a high current density of  $1000 \text{ mA g}^{-1}$  are shown in Fig. 4c. It should be pointed out that the cells were discharged and charged for 3 cycles at a low current density of  $100 \text{ mA g}^{-1}$  before cycle performance measurements. It can be seen that FGNs show a higher initial reversible specific capacity of  $633.6 \text{ mAh g}^{-1}$  than that of the RGNs ( $227.6 \text{ mAh g}^{-1}$ ) at the current density of  $1000 \text{ mA g}^{-1}$ . More significantly, even after 300 cycles, a reversible capacity of  $556.9 \text{ mAh g}^{-1}$  is maintained for the FGNs, which is still higher than the theoretical value of graphite ( $372 \text{ mAh g}^{-1}$ ) and the specific capacity for the RGNs ( $125.9 \text{ mAh g}^{-1}$ ). The cycle stability of the FGNs is superior to those of the graphene anode materials in the previous literature [1–8]. For example, the reversible specific capacity of graphene prepared by hydrazine reduction is decreased to  $460 \text{ mAh g}^{-1}$  after 100 cycles [4]. The excellent cycle performance could be ascribed to the stable structure between graphene nanosheets induced by the freeze-drying technology [25,28–30].

The rate capabilities and cycle performances of the FGNs and the RGNs at various current densities are shown in Fig. 4d. At a current density of  $100 \text{ mA g}^{-1}$ , the FGNs can be reversibly charge to  $1000.7 \text{ mAh g}^{-1}$  in the tenth cycle, which is much higher than that of the RGNs ( $321.7 \text{ mAh g}^{-1}$ ). Furthermore, with the current density was increased to 500, 1000, 2000, and  $3000 \text{ mA g}^{-1}$ , the corresponding reversible capacities are stabilized at 664, 519, 402, and  $342 \text{ mAh g}^{-1}$ , respectively. Most significantly, even at a very high current density of  $5000 \text{ mA g}^{-1}$ , a stable reversible capacity of  $275.3 \text{ mAh g}^{-1}$  could still be obtained, which is 3.5 times higher than the value for the RGNs electrode (about  $76.9 \text{ mAh g}^{-1}$ ). The rate capability of the FGNs also is also much better than that of previous report ( $445 \text{ mAh g}^{-1}$  at a high current density of  $1000 \text{ mA g}^{-1}$ ) [6]. More importantly, a specific capacity of  $939.9 \text{ mAh g}^{-1}$  can be recovered and stabilized when the current density is returned to the initial current density of  $100 \text{ mA g}^{-1}$ ,

suggesting that the as-obtained FGNs possess very good cycling stabilities. To better understand the improved rate performance, EIS measurements of the FGNs and RGNs were carried out before cycling and after 3 cycles. It is usually considered that the semicircle in the high/medium frequency range is assigned to the formation SEI film, contract resistance, and charge-transfer resistance, while the inclined line at an approximate  $45^\circ$  angle to the real axis corresponds to the lithium-diffusion process [2,10,16,18]. Obviously, the semicircle diameter of FGNs electrodes at high/medium frequency before and after cycling is smaller than that of RGNs electrodes, respectively (Fig. 4e and f). Thus, the FGNs electrodes show a higher electrical conductivity and a lower charge-transfer resistance compared with the RGNs electrodes.

Based on the above results, it is reasonable that the excellent electrochemical properties of the FGNs could be attributed to the following three factors. Firstly, the increased layer distance can provide more active sites for lithium-ion storage, which further increase the reversible specific capacity of graphene sheets [1]. Secondly, the high specific surface area can provide large electrode/electrolyte contact area and facilitate the transportation of lithium ions during the discharge/charge process. As a result, the rate capacities of graphene nanosheets as anodes for lithium-ion batteries could be enhanced. Thirdly, the stable structure constructed through freeze-drying process can improve the cycle stability of the graphene nanosheets. Therefore, the FGNs exhibit great electrochemical performance when used as anode materials, which make them as promising electrode materials for high-performance lithium-ion batteries.

#### 4. Conclusions

High-quality graphene nanosheets have been successfully prepared by a novel facile approach involving freeze-drying technology followed by thermal reduction. According to materials characterisation results, the FGNs possess larger interlayer distance and higher specific surface area than those of the RGNs. Consequently, the FGNs exhibit superior cycle stability ( $556.9 \text{ mAh g}^{-1}$  after 300 cycles at a high current density of  $1000 \text{ mA g}^{-1}$ ) and excellent rate capability ( $275.3 \text{ mAh g}^{-1}$  at a superhigh current density of  $5000 \text{ mA g}^{-1}$ ). The results demonstrate that the freeze-drying technology helps to improve the cycle stability and rate performance of graphene nanosheets. Moreover, the preparation method might give a rational direction to fabricate other highly

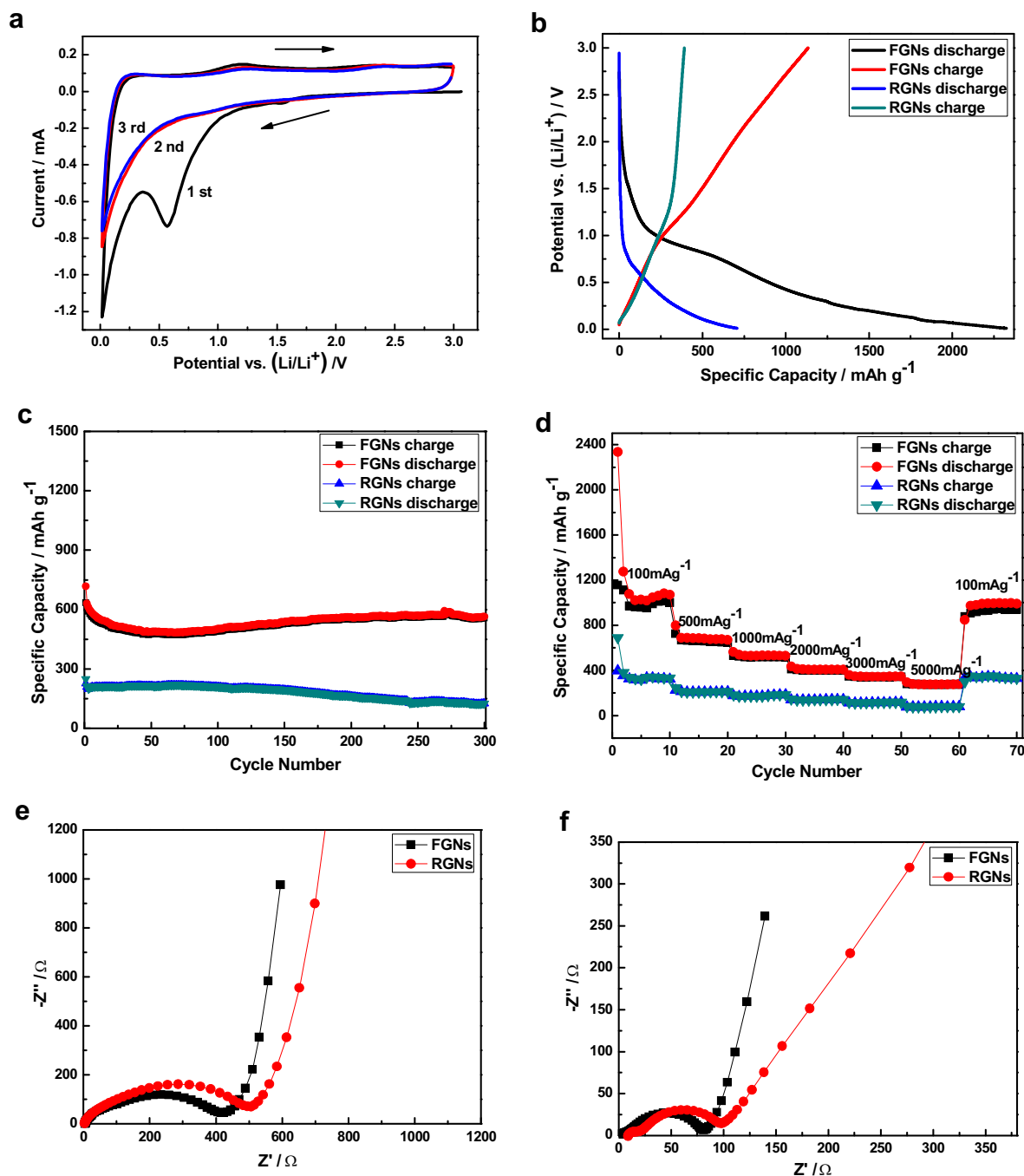


**Fig. 4.** (a) Cyclic voltammograms of the FGNs electrode, (b) Initial discharge/charge profiles of the FGNs and RGNs at a current density of  $100 \text{ mA g}^{-1}$ , (c) The cycling stabilities of the FGNs and RGNs at a high current density of  $1000 \text{ mA g}^{-1}$ , (d) The rate capabilities and cycle performances of the FGNs and the RGNs at various current densities, Nyquist plots of the FGNs and RGNs (e) before cycling and (f) after 3 cycles.

dispersed graphene-based materials for lithium-ion batteries, supercapacitor or lithium–air batteries.

#### Acknowledgements

This work was financially supported by National Science Fund for Distinguished Young Scholars of China (No. 21225625) and the National Natural Science Foundation of China (No. 21306057) and the Fundamental Research Funds for the Central Universities, SCUT (2013ZM0064).

#### References

- [1] E. Yoo, J. Kim, E. Hosono, H. Zhou, T. Kudo, I. Honma, *Nano Lett.* 8 (2008) 2277–2282.
- [2] P. Guo, H. Song, X. Chen, *Electrochem. Commun.* 11 (2009) 1320–1324.
- [3] D. Pan, S. Wang, B. Zhao, M. Wu, H. Zhang, Y. Wang, Z. Jiao, *Chem. Mater.* 21 (2009) 3136–3142.
- [4] G. Wang, X. Shen, J. Yao, J. Park, *Carbon* 47 (2009) 2049–2053.
- [5] C. Wang, D. Li, C.O. Too, G.G. Wallace, *Chem. Mater.* 21 (2009) 2604–2606.
- [6] P. Lian, X. Zhu, S. Liang, Z. Li, W. Yang, H. Wang, *Electrochim. Acta* 55 (2010) 3909–3914.
- [7] H. Xiang, Z. Li, K. Xie, J. Jiang, J. Chen, P. Lian, J. Wu, Y. Yu, H. Wang, *RSC Adv.* 2 (2012) 6792–6799.

- [8] R. Mukherjee, A.V. Thomas, A. Krishnamurthy, N. Koratkar, *ACS Nano* 6 (2012) 7867–7878.
- [9] J. Qiu, P. Zhang, M. Ling, S. Li, P. Liu, H. Zhao, S. Zhang, *ACS Appl. Mater. Interfaces* 4 (2012) 3636–3642.
- [10] X. Zhao, C.M. Harner, M.C. Kung, H. Kung, *ACS Nano* 11 (2011) 8739–8749.
- [11] S. Yin, Y. Zhang, J. Kong, C. Zou, C.M. Li, X. Lu, J. Ma, F.Y.C. Boey, X. Chen, *ACS Nano* 5 (2011) 3831–3838.
- [12] Y. Fang, Y. Lv, R. Che, H. Wu, X. Zhang, D. Gu, G. Zheng, D. Zhao, *J. Am. Chem. Soc.* 135 (2013) 1524–1530.
- [13] Z. Wang, D. Xu, H.G. Wang, Z. Wu, X. Zhang, *ACS Nano* 7 (2013) 2422–2430.
- [14] Z. Fan, J. Yan, G. Ning, T. Wei, L. Zhi, F. Wei, *Carbon* 60 (2013) 558–561.
- [15] A.L.M. Reddy, A. Srivastava, S.R. Gowda, H. Gullapalli, M. Dubey, P.M. Ajayan, *ACS Nano* 4 (2010) 6337–6342.
- [16] H. Wang, C. Zhang, Z. Liu, L. Wang, P. Han, H. Xu, K. Zhang, S. Dong, J. Yao, G. Cui, *J. Mater. Chem.* 21 (2011) 5430–5434.
- [17] X. Li, D. Geng, Y. Zhang, X. Meng, R. Li, X. Sun, *Electrochem. Commun.* 13 (2011) 822–825.
- [18] Z.S. Wu, W. Ren, L. Xu, F. Li, H.M. Cheng, *ACS Nano* 5 (2011) 5463–5471.
- [19] D. Cai, S. Wang, P. Lian, X. Zhu, D. Li, W. Yang, H. Wang, *Electrochim. Acta* 15 (2013) 492–497.
- [20] C. Zhang, N. Mahmood, H. Yin, F. Liu, Y. Hou, *Adv. Mater.* 25 (2013) 4932–4937.
- [21] H. Zhang, I. Hussain, M. Brust, M.F. Butler, S.P. Rannard, A.I. Cooper, *Nat. Mater.* 4 (2005) 787–793.
- [22] H. Zhang, A.I. Cooper, *Adv. Mater.* 19 (2007) 1529–1533.
- [23] J.L. Vickery, A.J. Patil, S. Mann, *Adv. Mater.* 21 (2009) 2180–2184.
- [24] H. Sun, Z. Xu, C. Gao, *Adv. Mater.* 25 (2013) 2554–2560.
- [25] Z.S. Wu, A. Winter, L. Chen, Y. Sun, A. Turchanin, X. Feng, K. Müllen, *Adv. Mater.* 24 (2012) 5130–5135.
- [26] S.J. Shi, J.P. Tu, Y.Y. Tang, Y.X. Yu, Y.Q. Zhang, X.L. Wang, *J. Power Sources* 221 (2013) 300–307.
- [27] S. Huang, Y. Lu, T.Q. Wang, C.D. Gu, X.L. Wang, J.P. Tu, *J. Power Sources* 235 (2013) 256–264.
- [28] L. Xiao, D. Wu, S. Han, Y. Huang, S. Li, M. He, F. Zhang, X. Feng, *Appl. Mater. Interfaces* 5 (2013) 3764–3769.
- [29] X. Zhou, Y.X. Yin, L.J. Wan, Y.G. Guo, *Chem. Commun.* 48 (2012) 2198–2200.
- [30] X. Zhou, L.J. Wan, Y.G. Guo, *Adv. Mater.* 25 (2013) 2152–2157.
- [31] A.K. Geim, K.S. Novoselov, *Nat. Mater.* 6 (2007) 183–191.
- [32] A.K. Geim, *Science* 324 (2009) 1530–1534.
- [33] D.R. Dreyer, S. Park, C.W. Bielawski, R.S. Ruoff, *Chem. Soc. Rev.* 39 (2010) 228–240.
- [34] X. Huang, K. Qian, J. Yang, J. Zhang, L. Li, C. Yu, D. Zhao, *Adv. Mater.* 24 (2012) 4419–4423.
- [35] M. Kruk, M. Jaronies, *Chem. Mater.* 13 (2001) 3169–3183.
- [36] S.M. Paek, E.J. Yoo, I. Honma, *Nano Lett.* 9 (2009) 72–75.
- [37] P.G. Bruce, B. Scrosati, J.M. Tarascon, *Angew. Chem. Int. Ed.* 47 (2008) 2930–2946.
- [38] K.T. Lee, J. Cho, *Nano Today* 6 (2011) 28–41.